A structural basis for inhibition of the complement initiator protease C1r by Lyme disease spirochetes

Ryan J. Garrigues[a], Alexandra D. Powell[b], Michal Hammel[c],

Jon T. Skare[b,*], and Brandon L. Garcia[a,*]

[a]Department of Microbiology and Immunology, Brody School of Medicine, East Carolina University, Greenville, North Carolina, United States of America

[b]Department of Microbial Pathogenesis and Immunology, College of Medicine, Texas A&M University, Bryan/College Station, Texas, United States of America

[c]Molecular Biophysics and Integrated Bioimaging, Lawrence Berkeley National Laboratory, Berkeley, CA, USA

Classification

BIOLOGICAL SCIENCES: Microbiology

Keywords

Complement system, *Borreliella burgdorferi*, complement evasion, small angle x-ray scattering, BBK32

Author Contributions

*These authors contributed equally to this work. Correspondence to Brandon L. Garcia (garciabr18@ecu.edu) and Jon T. Skare (jskare@tamu.edu).

J.T.S. and B.L.G. designed research; R.J.G., A.D.P., and M.H. performed research; R.J.G., A.D.P., M.H., J.T.S., and B.L.G. analyzed data; R.J.G., A.D.P., M.H., J.T.S, and B.L.G wrote the paper.

This PDF file includes:

Main Text
Figures 1 to 6
Table 1

Abstract

The complement system is a proteolytic cascade involving dozens of soluble and membrane-associated proteins that function in recognition, opsonization, and elimination of foreign or damaged cells of host origin. Complement evasion is a hallmark of certain human microbial pathogens such as *Borreliella burgdorferi*, the causative agent of Lyme disease, as well as related spirochetes. Lyme disease spirochetes express nearly a dozen outer surface lipoproteins that bind complement components and interfere with their native activities. Among these, BBK32 is unique in its selective inhibition of the classical pathway of complement. Previously we have shown that BBK32 blocks activation of this pathway by selectively binding and inhibiting the C1r serine protease subcomponent of the first component of complement, C1. To understand the structural basis for BBK32-mediated C1r inhibition, we performed size exclusion chromatography-coupled small angle x-ray scattering experiments, which revealed a molecular model of BBK32-C in complex with a truncated form of activated human C1r. Structure-guided site-directed mutagenesis was combined with surface plasmon resonance binding experiments and assays of complement function to validate the predicted molecular interface. Analysis of the structure shows that BBK32 inhibits C1r by occluding important substrate interaction subsites (i.e. S1 and S1') within the active site of C1r and reveals a surprising role for the C1r B loop in the BBK32 inhibitory model and overall C1r enzyme function. The studies reported here provide a structural basis for classical pathway-specific inhibition by a human pathogen and provide new insight into means for therapeutic inhibition of C1r in complement-related diseases.

Significance Statement

Complement is a major arm of the innate immune system, which functions in the recognition and destruction of pathogenic microbes. Bloodborne pathogens like the Lyme disease spirochete,

56 *Borreliella burgdorferi*, have evolved sophisticated mechanisms to evade complement-mediated
57 killing. In this study we provide a structural basis for how a complement inhibitor from *B.*
58 *burgdorferi,* designated BBK32, inhibits the initiating protease of the classical pathway of
59 complement, C1r. A molecular understanding for the unique complement inhibitory properties of
60 BBK32 improves our knowledge of how human pathogens combat one arm of the innate immune
61 response and reveals new ways to target C1r in complement-related autoimmune and inflammatory
62 diseases.
63
64

Introduction

The complement system consists of dozens of interacting soluble and surface-associated proteins that together form a primary arm of the innate immune system (1, 2). Activation of complement on a microbial surface leads to opsonization, recruitment of professional phagocytes, and in many cases, direct cellular lysis. Complement activation involves a cascading series of proteolytic reactions catalyzed by specialized serine proteases that cleave circulating inert complement components into activated fragments. The cascade can be initiated in multiple ways, leading to a canonical grouping of complement activation into three pathways known as the classical, lectin, and alternative pathways. The classical pathway is initiated by a multiprotein complex known as the first component of complement, C1. C1 is composed of C1q, two molecules of C1r, and two molecules of C1s ($C1qr_2s_2$). C1q serves as the pattern recognition molecule of the classical pathway, binding to immune complexes and non-antibody ligands resulting in zymogen activation of the attached C1r and C1s proteases. The lectin pathway is similarly initiated by pattern recognition, whereby mannan-binding lectin (MBL), ficolins, collectin-10 or collectin-11 bind foreign carbohydrate structures and cause activation of the MBL-associated proteases (MASPs). In contrast, the alternative pathway does not rely on pattern recognition but is instead continuously activated at a low level by a process known as 'tick-over'. All three initiating pathways converge at the cleavage of the central molecule of the cascade, complement component C3. C3 activation leads to formation of surface-bound enzyme complexes known as convertases that drive complement amplification and terminal pathway activation, ultimately resulting in the formation of the terminal pathway complete complex, C5b-9, also known as the membrane attack complex (MAC) (1, 2).

88 Complement activation is a finely tuned process controlled by endogenous regulators of
89 complement activity (RCAs) (3). RCAs are critical in preventing inappropriate complement
90 activation on the surface of healthy host cells. Indeed, aberrant activation or overactivation of
91 complement causes or exacerbates a wide range of human autoimmune, inflammatory, and
92 neurodegenerative diseases (4–6). Microbes lack RCAs and thus many human pathogens have
93 evolved sophisticated complement evasion systems to prevent complement-mediated attack (7). A
94 prototypical example of a bacterial complement evasion system is found in *Borreliella* spirochetes
95 (8, 9). *Borreliella* gen. nov. encompasses the etiological agents of Lyme disease including the
96 major genospecies *Borreliella burgdorferi, B. afzelii,* and *B. garinii* (10). The *Borreliella*
97 complement evasion repertoire is functionally overlapping and is categorized by two general
98 mechanisms (8, 9). The first mechanism involves functional recruitment of host RCAs to the
99 spirochete surface such as factor H (FH) (11–20). Among this group are the complement regulator
100 acquiring surface proteins (CRASPs) which include three distinct classes of FH-binding proteins
101 called CspA (CRASP-1), CspZ (CRASP-2), and three OspEF-related family paralogs known as
102 ErpP (CRASP-3), ErpC (CRASP-4), and ErpA (CRASP-5) (11–20). The second general
103 mechanism of complement evasion by outer surface *Borreliella* proteins involves a direct mode of
104 inhibition. Known inhibitors from this group include *B. bavariensis* BGA66 and BGA71 (21), a
105 FH-binding independent activity for CspA (22), and a protein of unknown molecular identity with
106 CD59-like activity that each interact with components of C5b-9 and prevent MAC formation (23).
107 In addition, two *Borreliella* outer surface lipoproteins are known to directly interfere with
108 upstream initiation steps of complement: OspC which binds to C4b and prevents classical/lectin
109 pathway proconvertase formation (24), and BBK32 which selectively blocks classical pathway
110 activation (25).

111 *B. burgdorferi* BBK32 is an outer surface-localized lipoprotein upregulated during the
112 vertebrate infection phase of the *B. burgdorferi* lifecycle (26). BBK32 is a multifunctional 47 kDa
113 protein with non-overlapping N-terminal binding sites for host glycosaminoglycans and
114 fibronectin (27, 28). Interactions by BBK32 with these molecules at the host endothelium are
115 cooperative and function to permit *B. burgdorferi* extravasation during hematogenous
116 dissemination (29, 30). More recently, we identified a potent complement inhibitory activity for
117 the C-terminal domain of BBK32 (BBK32-C, hereafter) (25). BBK32-C binds directly to the C1
118 complex and blocks the earliest proteolytic events of the classical pathway of complement (25).
119 The classical pathway-selective inhibitory activity of BBK32 – which arises due to its interaction
120 with the classical pathway-specific complex, C1 – is unique among known microbial complement
121 evasion proteins.

122 We have previously shown that BBK32-C binds the human C1 complex by specifically
123 recognizing the C1r subcomponent with high-affinity (25). Recently we obtained a high-resolution
124 crystal structure of BBK32-C and mapped its binding site on human C1r to the serine protease
125 (SP) domain (31). Collectively, these studies showed that BBK32-C is a noncovalent inhibitor of
126 C1r that is capable of blocking cleavage of both of its physiological substrates, notably, C1r itself
127 via autoactivation, as well as its partner protease in the C1 complex, C1s (25). However, the
128 structural basis and mechanism of action for BBK32-mediated C1r inhibition remains unknown.
129 To gain further insight into the nature of the BBK32/C1r protein-protein interaction, we carried
130 out a series of size exclusion chromatography coupled small angle x-ray scattering (SEC-SAXS)
131 experiments followed by a structure-guided mutagenesis strategy involving biophysical,
132 biochemical, and microbiological approaches. These investigations reveal the structural basis for
133 C1r inhibition by Lyme disease spirochetes, provide insight into BBK32's C1r selectivity, reveal

134 a convergent inhibitory mechanism between a spirochete and a hematophagous eukaryotic
135 organism, and uncover a previously unrecognized role for the B loop in C1r enzyme function.
136
137 **Results**
138
139 **The Solution Structure of the BBK32-C/C1r-CCP2-SP Complex.**
140 SAXS curves were obtained for recombinant BBK32-C (**Fig. S1, A, D**), a recombinant
141 autoactivated C1r domain truncation construct (hereafter, C1r-CCP2-SP) (**Fig. S1, B, E**), and an
142 equimolar mixture of BBK32-C and C1r-CCP2-SP (**Figs. 1A and S1C**). Radius of gyration (R_g)
143 values of 21.3, 24.0, and 27.8 Å were calculated from the Guinier region of the scattering curves
144 for BBK32-C, C1r-CCP2-SP, and BBK32-C/C1r-CCP2-SP samples, respectively (**Table 1**, **Figs.**
145 **1A, S1 D, E insets**). SAXS and multi-angle light scattering (MALS) determined molecular weights
146 (i.e., MW_{SAXS} and MW_{MALS}) are consistent with BBK32-C and C1r-CCP2-SP behaving as
147 monomeric species in solution (**Table 1**). For the BBK32-C/C1r-CCP2-SP sample MW_{SAXS} = 55.6
148 kDa (32) and MW_{MALS} = ~55-65 kDa were determined, which are close to the expected molecular
149 weight of a 1:1 complex ($MW_{sequence}$ = 54.6 kDa). Analysis of each scattering curve using a pair-
150 wise distribution function, P(r), is also consistent with complex formation as evidenced by the
151 shape of the overlaid P(r) profiles and increased maximum particle size (D_{max}) of the BBK32-
152 C/C1r-CCP2-SP samples relative to BBK32-C or C1r-CCP2-SP alone (**Fig. 1B, Table 1)**.

153 Next, we compared the solution state of each unbound protein to available high-resolution
154 crystal structures of BBK32-C (PDB: 6N1L (31)) and the activated form of C1r-CCP2-SP (PDB:
155 1MD8, (33)). First, MODELLER (34) as implemented in UCSF Chimera (35), was used to model
156 missing loops into each structure, and theoretical scattering profiles of each model were then
157 generated and compared against the raw scattering profiles using Fast X-ray Scattering (FoXS)
158 (36, 37). Good agreement between theoretical and experimental SAXS curves were obtained for

159 BBK32-C (χ = 2.08) and C1r-CCP2-SP (χ = 1.06) atomistic models (**Fig. S1 D, E Table 1**).
160 Collectively, analysis of the experimental SAXS curves strongly suggests that solution states of
161 unbound BBK32-C and activated C1r-CCP2-SP are in agreement with previously published
162 crystal structures and that BBK32-C/C1r-CCP2-SP forms a 1:1 stoichiometric complex in
163 solution.

164 To better define the molecular interface formed between BBK32 and human C1r, we employed
165 a SAXS-restrained macromolecular computational docking approach using FoXSDock (38). This
166 method – which relies on the availability of high-resolution structures of the individual complex
167 components – involves initial docking using a geometric shape-matching algorithm, coarse SAXS
168 filtering of the resulting docking models, scoring of the interface energies, and scoring the fit of
169 the model's theoretical SAXS profiles to the raw SAXS profile of the BBK32-C/C1r-CCP2-SP
170 complex (37). BBK32-C and C1r-CCP2-SP were docked as a ligand-receptor pair and each model
171 was compared against the BBK32-C/C1r-CCP2-SP SAXS curve. The top four models (as judged
172 by Z scores (38)), each exhibited nearly identical protein-protein interfaces involving BBK32-C
173 contact residues originating from helix 1, 5 and the short loop connecting helix 1 and 2. Consistent
174 with our previous mapping study (25), all C1r interactions in these four models involve only
175 residues within the C1r SP domain. We then reconstructed a molecular envelope using DAMMIF
176 (39, 40), which produced a distinctive chevron shape (**Figs. 1C,** gray envelope). Superimposition
177 of the top scoring FoxsDock model onto the shape envelope results in a close match, further
178 supporting the validity of the interface (**Fig. 1C**). Minimal molecular dynamics simulations using
179 BILBOMD (41) were performed on the best scoring model (χ = 1.28) to eliminate potential
180 clashes between side chains at the interface, further improving the model's SAX score (χ = 1.24)
181 (**Fig. 1C**).

182 **Analysis and Validation of the BBK32-C/C1r-CCP2-SP Structure**

183 Protein-protein interaction analysis was then carried out using the programs PISA and CCP4
184 CONTACT (42, 43). The model predicts an interaction between BBK32-C and C1r-CCP2-SP
185 involving 28 contact residues on the BBK32-C side and 34 contact residues from human C1r,
186 resulting in a total buried surface area (b.s.a.) of 1,270 $Å^2$ (**Fig. 2A**). To validate the predicted
187 interface, we carried out extensive structure-guided site-directed mutagenesis. A total of eleven
188 BBK32-C residues comprising > 50% of the total surface area buried by BBK32-C were changed
189 to alanine in single and/or double mutant forms. These mutants were then evaluated for direct
190 binding to C1r-CCP2-SP by surface plasmon resonance (SPR). Consistent with our previous SPR
191 binding measurements of BBK32-C for C1, C1r, proteolytic fragments of C1r, and HIS-tagged
192 recombinant domain truncations of C1r (25, 31), BBK32-C bound to activated C1r-CCP2-SP with
193 high affinity, exhibiting an equilibrium dissociation constant (K_D) of 0.5 nM (**Fig. 2B**). Three
194 different double alanine mutants involving mutagenesis of small contiguous contact surfaces, as
195 predicted by the SAXS structure, resulted in a 1,020-fold (K327A-T331A), 114-fold (T242A-
196 Y245A), and 960-fold (Y323A-E324A) reduction in affinity for C1r-CCP2-SP, whereas a fourth
197 such mutant retained an affinity similar to wild-type (L236A-T239A) (**Figs. 2B, S2-S3**). In the
198 case of T242A-Y245A and Y323A-E324A, single mutants retained wild-type-like affinity,
199 indicating that the observed affinity loss in the double mutants was due to a cumulative disruption
200 of a larger contact surface area (**Fig. 2B**). In contrast, a single K327A mutant resulted in a 240-
201 fold loss in affinity, whereas the paired T331A single mutant had near wild-type affinity (**Fig. 2B**).
202 Additional mutagenesis was directed at two charged residues predicted by the BBK32-C/C1r-
203 CCP2-SP structure to form sidechain-mediated hydrogen bonds (R248 and R337). While a single
204 R337A mutant exhibited wild-type like affinity, mutation of R248 resulted in a 12-fold loss in

205 affinity for C1r-CCP2-SP (**Fig. 2B, S2**). Although they do not form a contiguous binding surface,
206 a pairing of the two strongest loss-of-affinity single mutants (i.e., R248A-K327A), produced a
207 double mutant where no detectable binding signal was observed (**Fig. 2B**).

208 **R248 and K327 are Critical for BBK32-C Complement Inhibitory Activity**

209 Next we tested our panel of recombinant mutants for their ability to block serum-based
210 human complement activation in an ELISA assay that detects the classical pathway activation
211 product C4b. BBK32-C exhibited a half-maximal inhibitory concentration (IC_{50}) of 15 nM in this
212 assay format (**Fig. 3A, Table S1**), consistent with our previously reported value of 5.6 nM (25).
213 With the exception of E324A, which is discussed below, near wild-type IC_{50} values were measured
214 for BBK32-C mutants that retained high affinity for C1r-CCP2-SP, although we noted a modest
215 reduction in inhibitory activity in the Y245A (~5-fold), N251A (~6-fold) and Y323A (~2-fold)
216 single mutants (**Fig. S4 and Table S1**). Importantly, in all cases where mutants exhibited a strong
217 loss of affinity for C1r-CCP2-SP, they were also greatly impaired in their ability to block classical
218 pathway activation. For example, the contiguous surface double mutants Y323A-E324A and
219 K327A-T331A failed to block complement at any concentration, while a ~430-fold weaker IC_{50}
220 value for T242A-Y245A was measured (**Fig. S4 and Table S1**). Likewise, the R248A mutant was
221 attenuated ~28-fold, the K327A mutant did not block at the concentrations used, and the R248A-
222 K327A mutant was attenuated ~400-fold (**Figs. 3A, and Table S1**).

223 Based on the SAXS-derived BBK32-C/C1r-CCP2-SP structure we were able to identify
224 several BBK32 residues that mediate its binding and inhibitory activity, ultimately resulting in the
225 identification of two "hot-spot" residues, R248 and K327. To study the role of these two residues
226 in a more physiological setting, we produced site-directed BBK32 'knock-in' strains in the *B.*
227 *burgdorferi* B314 genetic background. *B. burgdorferi* B314 lacks linear plasmids that encode

228 many of the outer surface proteins associated with infection, including BBK32 (44, 45).
229 Previously we have shown that when wild-type BBK32 is expressed heterologously on the surface
230 of *B. burgdorferi* B314, it protects these normally serum-sensitive spirochetes from human
231 complement-mediated bacteriolysis (25, 31). Introduction of the R248A mutant into *B. burgdorferi*
232 B314 resulted in a minimal reduction in inhibitory activity relative to wild-type BBK32, while
233 spirochetes expressing K327A were significantly reduced in their sensitivity to human serum.
234 Spirochetes transformed with the *bbk32* R248A-K327A allele lost all protective activity and were
235 indistinguishable from the vector-only control (**Fig. 3B**). These data confirmed that the R248 and
236 K327 residues are critical for eliciting complement inhibitory activity in the context of full-length
237 BBK32 on the outer surface of *B. burgdorferi*. Western immunoblots showed that full length
238 BBK32 was produced equivalently in all mutants tested, indicating that the enhanced sensitivity
239 of the R248-K327A double mutant was not the result of proteolytic instability (**Fig S5**). The
240 functional importance of these residues is further supported by the complete loss of inhibitory
241 activity by recombinant BBK32-R248A-K327A in an enzymatic assay that monitors the
242 proteolytic activation of a natural C1r substrate, proenzyme C1s, by purified full-length C1r
243 enzyme (**Fig. 3C**).

244 **BBK32 Occludes Subsites Within the Active Site of C1r**

245 Having taken steps to validate the SAXS-derived structural model, and in so doing, identifying
246 key interactions that mediate BBK32-C/C1r-CCP2-SP complex formation, we then analyzed the
247 structure for potential clues into the mechanism of C1r inhibitory action by BBK32. C1r is a
248 modular serine protease with a chymotrypsin-like SP domain (46). We noted that the BBK32
249 binding site on human C1r is in close proximity to the C1r catalytic site (**Fig. 4A**). Although limited
250 contacts are made in the model with active site residues (28 $Å^2$ b.s.a.), much more extensive

251 interactions are made with the specificity pocket subsites S1 (176 Å^2 b.s.a.) and S1' (167 Å^2 b.s.a.)
252 (**Fig. 4B**). Residues involved in S1 (red) and S1' (blue) subsite interactions were mapped onto the
253 BBK32-C surface (**Fig. 4B**). These include three residues (T242, Y245, and R248) that were
254 shown to have loss of function effects when mutated to alanine (**Figs. 2-3**). The steric occlusion
255 of the S1 and S1' site by BBK32 predicts that it would be capable of blocking the hydrolysis of
256 small peptide C1r substrates. To examine this, we assayed C1r-CCP2-SP cleavage of a
257 colorimetric peptide substrate that requires only P2-P1-P1' access (i.e. Z-Gly-Arg-thiobenzyl) in
258 the presence of increasing concentrations of inhibitor. BBK32-C, but not the negative control (i.e.
259 BBK32-R248A-K327A), dose-dependently blocked cleavage of this small substrate (**Fig. 4C**).

260 **BBK32-C Targets Non-Conserved C1r Loops Outside of the Active Site**

261 We have previously shown that BBK32 is highly selective for C1r binding relative to C1s
262 (25). Sequence alignment of the SP domains of C1r and C1s reveal that 25 of the 34 human C1r
263 contact residues in the BBK32-C/C1r-CCP2-SP SAXS structure are non-identical in C1s (**Fig. 5**).
264 Most of these differences arise from contacts involving the S1' site and four C1r loops (i.e. A, B,
265 D, E loops), suggesting these interactions may underly the selectivity of BBK32 for C1r. To gain
266 further insight into this possibility, we compared the interface of BBK32-C/C1r-CCP2-SP present
267 in the SAXS structure to that of a previously published structure of a protein inhibitor of both the
268 classical and lectin complement pathways known as gigastasin (47). Gigastasin is produced by the
269 giant Amazonian leech (*Haementeria ghilianii*), but it differs in selectivity from BBK32 as it
270 blocks C1s, MASP-1 and MASP-2, but is a relatively weak inhibitor of C1r (47). Interestingly, the
271 gigastasin/C1s protein-protein interface shares common features with the BBK32-C/C1r-CCP2-
272 SP SAXS structure presented here. Namely, both inhibitors form extensive interactions with the
273 S1 and S1' subsites of their respective target enzymes. Furthermore, BBK32 and gigastasin both

274 interact with the A, D, and E loops as well as loop 2 (**Fig. 5**). Given the vastly different three-
275 dimensional structures of BBK32 and gigastasin (**Fig. 5**), it appears that a bloodborne prokaryote
276 (*B. burgdorferi*) and a blood-feeding eukaryote (*H. ghilianii*) have evolved complement inhibitors
277 with convergent mechanisms of action.

278 **BBK32 Forms Extensive Interactions with the C1r B loop**

279 Despite the common features of BBK32 and gigastasin described above, we also noted that
280 BBK32 is unique in that it makes extensive interactions with the B loop of C1r. This loop contains
281 an insertion sequence making it longer in C1r compared to most other complement serine
282 proteases, including C1s (**Fig. 5**). Of the 16 residues that comprise the C1r B loop, 10 form contacts
283 with BBK32-C. Of these 10 contact residues, none are identical at the homologous position in C1s
284 (**Fig. 5**). In the BBK32-C/C1r-CCP2-SP SAXS structure, the B loop sits directly across from the
285 small kinked region of alpha helix 5 on BBK32, where K327 resides (**Fig. 6A**). Mutation of K327
286 to alanine resulted in our most severe loss of function for a single mutant in *in vitro* biochemical
287 assays (**Figs. 2 and 3**), underscoring the critical nature of the BBK32-C/C1r-CCP2-$SP_{B\ loop}$
288 interface in driving both affinity and inhibitory activity of BBK32. To investigate this further, we
289 produced a construct of C1r-CCP2-SP where the three B loop residues in closest proximity to
290 BBK32-K327 were changed to alanine (i.e. N514A-S516A-D518A) (**Fig. 6A**). Interestingly, this
291 mutant resulted in only a two-fold reduction in affinity (K_D) for BBK32-C owed to a decreased
292 association rate constant (k_a), whereas the dissociation rate constant (k_d) was similar to that of wild-
293 type C1r-CCP2-SP (**Fig. 6B, Table S1**). This finding suggests that BBK32-K327 may form
294 compensatory interactions with this mutant. Nonetheless, these data collectively indicate that
295 interactions made by BBK32 outside of the C1r active site are important to its inhibitory activity.

296 **Residues in the C1r B loop are Important for C1r Function**

297 A role for the B loop in C1r function has not been previously described. However, the
298 extensive interactions formed with this relatively unique region of C1r by an evolutionarily
299 optimized inhibitor like BBK32, suggested it may be important to the enzymatic function of C1r.
300 To test this hypothesis, we measured the ability of our C1r-CCP2-SP B loop mutant (i.e. N514A-
301 S516A-D518A) to activate a natural substrate, proenzyme C1s, by comparing its activity to C1r-
302 CCP2-SP wild-type enzyme. In two different assay formats of proenzyme C1s cleavage, we found
303 that the C1r-CCP2-SP-N514A-S516A-D518A mutant protein was significantly impaired in its
304 ability to cleave proenzyme C1s (**Figs. 6C, D**). These data support the idea that residues residing
305 outside of the C1r active site, notably B loop residues, are important to its role as the initiator
306 protease of the classical pathway.

307 **Discussion**
308

309 In the absence of regulation, complement activation at the microbial surface leads to
310 deposition of C3b or C4b on the microbe surface, opsonization by innate immune cells due to the
311 presence of immobilized C3b and C4b, potent recruitment of leukocytes by the anaphylatoxins
312 C3a and C5a, stimulation of the adaptive immune response by each of these fragments, and direct
313 bactericidal action by C5b-9 (i.e., MAC) (1, 2). While intracellular pathogens may be protected by
314 complement within an intracellular niche, extracellular pathogens like *Borreliella* spirochetes face
315 a continuous threat from the complement systems of their hosts. *Borreliella* first encounter
316 complement during the bloodmeal of an infected *Ixodes* sp. tick. Following transmission from their
317 arthropod vector into the vertebrate host, spirochetes must continue to protect themselves from
318 complement during hematogenous dissemination, a challenge that persists once they colonize
319 distant tissues. To evade complement attack, Lyme disease spirochetes express nearly a dozen

320 different outer surface lipoproteins that directly interact with complement proteins and modulate
321 their native activities (8, 9).

322 Like Lyme disease spirochetes, other bloodborne pathogens and blood feeding eukaryotes
323 have evolved complement evasion systems. For example, potent direct inhibitors of complement
324 are produced in the salivary glands of several species of ticks, including *Ixodes* sp. (48–52).
325 Similarly, blood-feeding insects like sandflies (53) and mosquitos (54), along with other human
326 bacterial pathogens such as *Staphylococcus aureus* (7, 55, 56), all produce a wide array of
327 mechanistically distinct protein inhibitors of the complement cascade. However, among known
328 complement evasion molecules, relatively few target the classical pathway with specificity, and to
329 our knowledge BBK32 remains the only reported macromolecule of natural origin that selectively
330 blocks C1r (56). Despite this, our study identifies a surprising convergence of function between
331 *B. burgdorferi* BBK32 and a complement protease inhibitor of the classical and lectin pathways
332 previously identified in the giant Amazonian leech (i.e. gigastasin). Each inhibitor functions, at
333 least in part, by steric occlusion of the subsites upon enzyme-inhibitor complex formation (47). A
334 major difference between the gigastasin and BBK32 enzyme-inhibitor complexes involve
335 interactions made by BBK32 with the C1r B loop, which appear to underly BBK32's C1r
336 selectivity over other closely related complement proteases such as C1s (**Fig. 5**).

337 Our study suggests that BBK32 inhibits human C1r by simultaneously targeting its active site,
338 as well as functionally critical non-active site, residues. For example, BBK32 residue R248 –
339 which binds to the C1r S1 subsite – serves as a prototypical example of BBK32's active site
340 targeted inhibitory mode (**Figs. 2-4**). Separate from these active site targeting residues, we also
341 identified an important interaction involving non-active site residues on the C1r B loop with
342 residues from the fifth alpha helix of BBK32 (i.e., K327) (**Figs. 2, 3, 6B**). While the functional

343 role of the B loop in C1r is not well understood, we showed here that it is important in C1r enzyme
344 function (**Fig. 6C, D**). The increased length of the B loop in C1r is unique to a select group of
345 chymotrypsin-like serine proteases, including the coagulation cascade protease thrombin, where it
346 functions as a determinant of substrate specificity (57). Intriguingly, studies involving B loop
347 deletion mutants of thrombin have revealed a critical role for this loop in substrate recognition
348 (58). Whether this is also the case for C1r requires more study.

349 We note that a prerequisite for potent BBK32-mediated inhibition is high-affinity interaction
350 with C1r, as evidenced by a strong reduction in activity by all loss-of-affinity mutants tested here.
351 However, a curious exception to this expected high-affinity/high-potency relationship is BBK32-
352 E324A. This mutant was reduced only three-fold in affinity for C1r-CCP2-SP (**Fig. 2**), but by
353 several orders of magnitude in inhibitory activity (**Fig. S4**). BBK32-E324 is located next to K327
354 on the face of alpha helix 5 of BBK32 and, like K327, forms contacts with the C1r B loop. In our
355 previous study we coincidentally probed the function of this residue position while investigating
356 the reduced complement inhibitory activity of a BBK32 homologue from *B. garinii*, termed
357 BGD19 (31). In that study, a triple mutant chimeric recombinant protein termed BXK32-C was
358 created to convert BBK32 to BGD19 at three non-conserved residue positions (i.e., BBK32-
359 E308K-Q319K-E324Q) (31). This mutant shifted from BBK32-like to BGD19-like inhibitory
360 activity, leading us to conclude that at least one of these three surface-exposed residues was
361 important for the complement inhibitory activity of BBK32. Among the three residues in the
362 BXK32 mutant, only E324 is a contact residue in the BBK32-C/C1r-CCP2-SP SAXS structure.
363 Similar to the activity reported here for BBK32-E324A, recombinant BGD19 and BXK32 retained
364 high affinity for human C1r while having a greatly reduced inhibitory activity. While the
365 underlying reasons for the disconnect between the binding and inhibitory activities of these

366 proteins remain unclear, these data suggest that specific conformations of the B loop may be
367 important for C1r function. Furthermore, given that mutants like BBK32-E324A retain all of the
368 necessary physicochemical information to target the active site (i.e. R248, etc.), these data suggest
369 that the ability of BBK32 to target the active site is necessary but not sufficient to attain its full
370 inhibitory activity.

371 Interestingly, genospecies of *Borreliella* vary widely in their susceptibility to serum-based
372 complement-mediated bacteriolysis (59). While the categorizations are general and not without
373 exceptions, *B. burgdorferi* is typically considered serum-resistant whereas *B. garinii* is susceptible
374 to killing by human serum. The overall susceptibility of a spirochete to a particular host
375 complement system is related to the collective activities of the larger *Borreliella* complement
376 evasion system (i.e., CRASPs, OspC, BBK32, etc.). However, insight into this host association
377 phenomenon may be gained from analysis of a single *Borreliella* complement inhibitor, in this
378 case BBK32. Our original analysis of *B. garinii* BGD19, discussed above, implicated three
379 differentially encoded residues in BGD19 likely involved in its activity difference relative to
380 BBK32. Here we have pinpointed the likely cause of the reduced BGD19 activity to a single
381 contact residue in the BBK32/C1r-CCP2-SP structure, residue position E324. Unlike R248 and
382 K327, which drive human C1r affinity and are universally conserved across publicly available *B.*
383 *burgdorferi* genome sequences, position 324 is less conserved (**Fig. S6**). We speculate that
384 variation in position 324 in naturally occurring BBK32 sequences may allow for optimal inhibition
385 of C1r in other vertebrates as the sequence of the C1r B loop is one of the least conserved features
386 within vertebrate C1r. Further studies, including high-resolution structural information involving
387 synthetic or naturally occurring BBK32 sequences such as *B. garinii* BGD19, along with

388 mechanistic studies involving targeted C1r B loop mutants, will be needed to further test this
389 possibility.

390 C1r's role as the initiator protease of the classical pathway remains its only known
391 physiological function. Aberrant activation of the classical pathway has been linked to a wide
392 range of human autoimmune and inflammatory conditions, and C1r presents a promising target for
393 classical pathway-specific therapeutic interventions (6, 60, 61). Given that BBK32-mediated C1r
394 inhibition has arisen *in vivo* from evolutionary pressure at the host-pathogen interface, a drug-like
395 molecule with a BBK32-like inhibitory mode holds promise for the development of selective and
396 potent complement-directed drugs. As such, the structure of the BBK32/C1r-CCP2-SP complex
397 provides new insight into the development of highly selective C1r inhibitors. Selective targeting
398 of the C1r subsites, as is seen for BBK32 residues like R248, may be difficult to achieve given the
399 large potential for off-target effects for closely related complement proteases or other blood serine
400 proteases such as those of the coagulation cascade. However, the work presented here shows that
401 selective inhibition might be achieved by targeting of loop structures unique to C1r, in particular
402 the C1r B loop.

403 For the first time, this study provides a structural basis for classical pathway complement
404 evasion by a human pathogen. Among naturally occurring complement inhibitors *B. burgdorferi*
405 BBK32 is unique in its ability to selectively target and inhibit the initiator protease of the classical
406 pathway, C1r, and, as such, the structure-function studies reported here provide new insight into
407 an evolutionarily optimized mechanism of action for C1r inhibition. This knowledge improves our
408 understanding of complement evasion in Lyme spirochetes, increases our understanding of
409 naturally occurring complement inhibitors, and provides a basis for the development of novel
410 complement directed therapeutics that are classical pathway-specific.

411 **Materials and Methods**

412 Strains, plasmids, and oligonucleotides used in this study are reported in **Table S2**. Culture
413 conditions, protein expression and purification protocols, immunoblotting, SPR, and complement
414 inhibition assays were performed as described in *SI Appendix* and *SI Materials and Methods*.
415 Details on SEC-SAXS-MALS, including sample preparation, data collection, and data processing
416 are provided in *SI Appendix and SI Materials and Methods*. All statistical analysis is reported in
417 *SI Materials and Methods.*

418 **Data Availability**

419 SAXS data and models are deposited in the Small Angle Scattering Biological Data Bank
420 (www.sasdb.org) with accession codes SASDKX7 (BBK32-C/C1r-CCP2-SP), SASDKV7 (C1r-
421 CCP2-SP), and SASDKW7 (BBK32-C).

422 **Acknowledgments**

423 SAXS data was collected at SIBYLS which is supported by the DOE-BER IDAT DE-AC02-
424 05CH11231 and NIGMS ALS-ENABLE (P30 GM124169 and S10OD018483). This work was
425 supported by Public Health Service Grants AI133367 and AI146930 (to JTS and BLG).

426

427 **References**

428 1. N. S. Merle, S. E. Church, V. Fremeaux-Bacchi, L. T. Roumenina, Complement System
429 Part I - Molecular Mechanisms of Activation and Regulation. *Front. Immunol.* **6**, 262
430 (2015).

431 2. N. S. Merle, R. Noe, L. Halbwachs-Mecarelli, V. Fremeaux-Bacchi, L. T. Roumenina,
432 Complement System Part II: Role in Immunity. *Front. Immunol.* **6**, 257 (2015).

433 3. C. Q. Schmidt, J. D. Lambris, D. Ricklin, Protection of host cells by complement
434 regulators. *Immunol. Rev.* **274**, 152–171 (2016).

435 4. D. Ricklin, J. D. Lambris, Complement in immune and inflammatory disorders:
436 pathophysiological mechanisms. *J. Immunol. (Baltimore, Md. 1950)* **190**, 3831–3838
437 (2013).

438 5. B. P. Morgan, Complement in the pathogenesis of Alzheimer's disease. *Semin.*
439 *Immunopathol.* **40**, 113–124 (2018).

440 6. D. Ricklin, D. C. Mastellos, E. S. Reis, J. D. Lambris, The renaissance of complement
441 therapeutics. *Nat. Rev. Nephrol.* **14**, 26–47 (2018).

442 7. J. D. Lambris, D. Ricklin, B. V Geisbrecht, Complement evasion by human pathogens.
443 *Nat. Rev. Microbiol.* **6**, 132–142 (2008).

444 8. P. Kraiczy, Hide and Seek: How Lyme Disease Spirochetes Overcome Complement
445 Attack. *Front. Immunol.* **7**, 385 (2016).

446 9. J. T. Skare, B. L. Garcia, Complement Evasion by Lyme Disease Spirochetes. *Trends*
447 *Microbiol.* (2020) https:/doi.org/10.1016/j.tim.2020.05.004.

448 10. M. Adeolu, R. S. Gupta, A phylogenomic and molecular marker based proposal for the
449 division of the genus *Borrelia* into two genera: the emended genus *Borrelia* containing
450 only the members of the relapsing fever *Borrelia*, and the genus *Borreliella* gen. nov.
451 containing the members o. *Antonie Van Leeuwenhoek* **105**, 1049–1072 (2014).

452 11. P. Kraiczy, *et al.*, Complement resistance of *Borrelia* burgdorferi correlates with the
453 expression of BbCRASP-1, a novel linear plasmid-encoded surface protein that interacts
454 with human factor H and FHL-1 and is unrelated to Erp proteins. *J. Biol. Chem.* **279**,
455 2421–2429 (2004).

456 12. K. Hartmann, *et al.*, Functional characterization of BbCRASP-2, a distinct outer
457 membrane protein of *Borrelia burgdorferi* that binds host complement regulators factor H
458 and FHL-1. *Mol. Microbiol.* **61**, 1220–1236 (2006).

459 13. B. Stevenson, K. Tilly, P. A. Rosa, A family of genes located on four separate 32-kilobase
460 circular plasmids in *Borrelia burgdorferi* B31. *J. Bacteriol.* **178**, 3508–3516 (1996).

461 14. B. Stevenson, N. El-Hage, M. A. Hines, J. C. Miller, K. Babb, Differential binding of host
462 complement inhibitor factor H by *Borrelia burgdorferi* Erp surface proteins: A possible
463 mechanism underlying the expansive host range of Lyme disease spirochetes. *Infect.*
464 *Immun.* (2002) https:/doi.org/10.1128/IAI.70.2.491-497.2002.

465 15. J. V McDowell, *et al.*, Comprehensive analysis of the factor h binding capabilities of
466 borrelia species associated with lyme disease: delineation of two distinct classes of factor
467 h binding proteins. *Infect. Immun.* **71**, 3597–3602 (2003).

468 16. J. V McDowell, *et al.*, Evidence that the BBA68 protein (BbCRASP-1) of the Lyme
469 disease spirochetes does not contribute to factor H-mediated immune evasion in humans
470 and other animals. *Infect. Immun.* **74**, 3030–3034 (2006).

471 17. T. Bykowski, *et al.*, *Borrelia burgdorferi* complement regulator-acquiring surface proteins
472 (BbCRASPs): Expression patterns during the mammal-tick infection cycle. *Int. J. Med.*
473 *Microbiol. IJMM* **298 Suppl**, 249–256 (2008).

474 18. M. R. Kenedy, S. R. Vuppala, C. Siegel, P. Kraiczy, D. R. Akins, CspA-mediated binding
475 of human factor H inhibits complement deposition and confers serum resistance in
476 *Borrelia burgdorferi*. *Infect. Immun.* **77**, 2773–2782 (2009).

477 19. E. A. Rogers, S. V Abdunnur, J. V McDowell, R. T. Marconi, Comparative analysis of the
478 properties and ligand binding characteristics of CspZ, a factor H binding protein, derived
479 from *Borrelia burgdorferi* isolates of human origin. *Infect. Immun.* **77**, 4396–4405 (2009).

480 20. M. R. Kenedy, D. R. Akins, The OspE-related proteins inhibit complement deposition and
481 enhance serum resistance of *Borrelia burgdorferi*, the lyme disease spirochete. *Infect.*
482 *Immun.* **79**, 1451–1457 (2011).

483 21. C. Hammerschmidt, *et al.*, BGA66 and BGA71 facilitate complement resistance of
484 *Borrelia bavariensis* by inhibiting assembly of the membrane attack complex. *Mol.*
485 *Microbiol.* **99**, 407–424 (2016).

486 22. T. Hallström, *et al.*, CspA from *Borrelia burgdorferi* inhibits the terminal complement
487 pathway. *MBio* **4**, 13 (2013).

488 23. M. Pausa, *et al.*, Serum-resistant strains of *Borrelia burgdorferi* evade complement-
489 mediated killing by expressing a CD59-like complement inhibitory molecule. *J. Immunol.*
490 *(Baltimore, Md. 1950)* **170**, 3214–3222 (2003).

491 24. J. A. Caine, *et al.*, *Borrelia burgdorferi* outer surface protein C (OspC) binds complement
492 component C4b and confers bloodstream survival. *Cell. Microbiol.* **19** (2017).

493 25. B. L. Garcia, H. Zhi, B. Wager, M. Höök, J. T. Skare, *Borrelia burgdorferi* BBK32
494 Inhibits the Classical Pathway by Blocking Activation of the C1 Complement Complex.
495 *PLoS Pathog.* **12**, e1005404 (2016).

496 26. M. He, B. K. Boardman, D. Yan, X. F. Yang, Regulation of expression of the fibronectin-
497 binding protein BBK32 in *Borrelia burgdorferi*. *J. Bacteriol.* **189**, 8377–8380 (2007).

498 27. W. S. Probert, J. H. Kim, M. Höök, B. J. Johnson, Mapping the ligand-binding region of
499 *Borrelia burgdorferi* fibronectin-binding protein BBK32. *Infect. Immun.* **69**, 4129–4133
500 (2001).

501 28. J. R. Fischer, K. T. LeBlanc, J. M. Leong, Fibronectin binding protein BBK32 of the
502 Lyme disease spirochete promotes bacterial attachment to glycosaminoglycans. *Infect.*
503 *Immun.* **74**, 435–441 (2006).

504 29. T. J. Moriarty, *et al.*, Vascular binding of a pathogen under shear force through
505 mechanistically distinct sequential interactions with host macromolecules. *Mol. Microbiol.*
506 **86**, 1116–1131 (2012).

507 30. R. Ebady, *et al.*, Biomechanics of *Borrelia burgdorferi* Vascular Interactions. *Cell Rep.*
508 **16**, 2593–2604 (2016).

509 31. J. Xie, *et al.*, Structural determination of the complement inhibitory domain of *Borrelia*
510 *burgdorferi* BBK32 provides insight into classical pathway complement evasion by Lyme
511 disease spirochetes. *PLoS Pathog.* **15**, e1007659 (2019).

512 32. R. P. Rambo, J. A. Tainer, Accurate assessment of mass, models and resolution by small-
513 angle scattering. *Nature* (2013) https:/doi.org/10.1038/nature12070.

514 33. M. Budayova-Spano, *et al.*, Monomeric structures of the zymogen and active catalytic
515 domain of complement protease c1r: further insights into the c1 activation mechanism.
516 *Struct. (London, Engl. 1993)* **10**, 1509–1519 (2002).

517 34. B. Webb, A. Sali, Comparative protein structure modeling using MODELLER. *Curr.*
518 *Protoc. Bioinforma.* **2014**, 5.6.1-5.6.32 (2014).

519 35. E. F. Pettersen, *et al.*, UCSF Chimera - A visualization system for exploratory research
520 and analysis. *J. Comput. Chem.* **25**, 1605–1612 (2004).

521 36. D. Schneidman-Duhovny, M. Hammel, J. A. Tainer, A. Sali, Accurate SAXS profile
522 computation and its assessment by contrast variation experiments. *Biophys. J.* **105**, 962–
523 974 (2013).

524 37. D. Schneidman-Duhovny, M. Hammel, J. A. Tainer, A. Sali, FoXS, FoXSDock and
525 MultiFoXS: Single-state and multi-state structural modeling of proteins and their
526 complexes based on SAXS profiles (2016).

527 38. D. Schneidman-Duhovny, M. Hammel, A. Sali, Macromolecular Docking Restrained by a
528 Small Angle X-Ray Scattering Profile (2010) https:/doi.org/10.1016/j.jsb.2010.09.023.

529 39. D. Franke, D. I. Svergun, DAMMIF, a program for rapid ab-initio shape determination in
530 small-angle scattering. *J. Appl. Crystallogr.* (2009)
531 https:/doi.org/10.1107/S0021889809000338.

532 40. V. V. Volkov, D. I. Svergun, Uniqueness of ab initio shape determination in small-angle
533 scattering in *Journal of Applied Crystallography*, (2003)
534 https:/doi.org/10.1107/S0021889803000268.

535 41. M. Pelikan, G. L. Hura, M. Hammel, Structure and flexibility within proteins as identified
536 through small angle X-ray scattering. *Gen. Physiol. Biophys.* (2009)
537 https:/doi.org/10.4149/gpb_2009_02_174.

538 42. M. D. Winn, *et al.*, Overview of the CCP4 suite and current developments. *Acta*
539 *Crystallogr. Sect. D Biol. Crystallogr.* (2011)
540 https:/doi.org/10.1107/S0907444910045749.

541 43. E. Krissinel, K. Henrick, Inference of Macromolecular Assemblies from Crystalline State.

542 *J. Mol. Biol.* **372**, 774–797 (2007).

543 44. A. Sadziene, B. Wilske, M. S. Ferdows, A. G. Barbour, The cryptic ospC gene of *Borrelia*
544 *burgdorferi* B31 is located on a circular plasmid. *Infect. Immun.* **61**, 2192–2195 (1993).

545 45. A. Sadziene, D. D. Thomas, A. G. Barbour, *Borrelia burgdorferi* mutant lacking Osp:
546 biological and immunological characterization. *Infect. Immun.* **63**, 1573–1580 (1995).

547 46. J. Kardos, *et al.*, The Role of the Individual Domains in the Structure and Function of the
548 Catalytic Region of a Modular Serine Protease, C1r. *J. Immunol.* **167**, 5202–5208 (2001).

549 47. S. S. Pang, *et al.*, The Structural Basis for Complement Inhibition by Gigastasin, a
550 Protease Inhibitor from the Giant Amazon Leech. *J. Immunol. (Baltimore, Md. 1950)* **199**,
551 3883–3891 (2017).

552 48. M. P. Reichhardt, *et al.*, An inhibitor of complement C5 provides structural insights into
553 activation. *Proc. Natl. Acad. Sci. U. S. A.* (2020) https:/doi.org/10.1073/pnas.1909973116.

554 49. K. Tyson, C. Elkins, H. Patterson, E. Fikrig, A. de Silva, Biochemical and functional
555 characterization of Salp20, an Ixodes scapularis tick salivary protein that inhibits the
556 complement pathway. *Insect Mol. Biol.* **16**, 469–479 (2007).

557 50. T. J. Schuijt, *et al.*, The tick salivary protein Salp15 inhibits the killing of serum-sensitive
558 *Borrelia burgdorferi* sensu lato isolates. *Infect. Immun.* (2008)
559 https:/doi.org/10.1128/IAI.00232-08.

560 51. N. C. S. Silva, *et al.*, Saliva of Rhipicephalus (Boophilus) microplus (Acari: Ixodidae)
561 inhibits classical and alternative complement pathways. *Parasites and Vectors* (2016)
562 https:/doi.org/10.1186/s13071-016-1726-8.

563 52. T. J. Schuijt, *et al.*, A tick mannose-binding lectin inhibitor interferes with the vertebrate
564 complement cascade to enhance transmission of the lyme disease agent. *Cell Host*
565 *Microbe* **10**, 136–146 (2011).

566 53. V. P. Ferreira, *et al.*, SALO, a novel classical pathway complement inhibitor from saliva
567 of the sand fly *Lutzomyia longipalpis*. *Sci. Rep.* (2016) https:/doi.org/10.1038/srep19300.

568 54. A. F. Mendes-Sousa, *et al.*, An Inhibitor of the Alternative Pathway of Complement in
569 Saliva of New World Anopheline Mosquitoes. *J. Immunol.* (2016)
570 https:/doi.org/10.4049/jimmunol.1600020.

571 55. B. L. Garcia, K. X. Ramyar, D. Ricklin, J. D. Lambris, B. V Geisbrecht, Advances in
572 understanding the structure, function, and mechanism of the SCIN and Efb families of
573 Staphylococcal immune evasion proteins. *Adv. Exp. Med. Biol.* **946**, 113 (2012).

574 56. B. L. Garcia, S. A. Zwarthoff, S. H. M. Rooijakkers, B. V Geisbrecht, Novel Evasion
575 Mechanisms of the Classical Complement Pathway. *J. Immunol.* **197**, 2051–2060 (2016).

576 57. M. J. Page, R. T. A. Macgillivray, E. Di Cera, Determinants of specificity in coagulation
577 proteases. *J. Thromb. Haemost.* (2005) https:/doi.org/10.1111/j.1538-7836.2005.01456.x.

578 58. A. R. Rezaie, L. Yang, Deletion of the 60-loop provides new insights into the substrate
579 and inhibitor specificity of thrombin. *Thromb. Haemost.* (2005)

580 https:/doi.org/10.1160/TH04-11-0730.

581 59. P. Kraiczy, Travelling between Two Worlds: Complement as a Gatekeeper for an
582 Expanded Host Range of Lyme Disease Spirochetes. *Vet. Sci.* **3** (2016).

583 60. D. C. Mastellos, D. Ricklin, J. D. Lambris, Clinical promise of next-generation
584 complement therapeutics. *Nat. Rev. Drug Discov.* (2019) https:/doi.org/10.1038/s41573-
585 019-0031-6.

586 61. C. L. Harris, R. B. Pouw, D. Kavanagh, R. Sun, D. Ricklin, Developments in anti-
587 complement therapy; from disease to clinical trial. *Mol. Immunol.* **102**, 89–119 (2018).

588 62. I. Schechter, A. Berger, On the size of the active site in proteases. I. Papain. *Biochem.*
589 *Biophys. Res. Commun.* (1967) https:/doi.org/10.1016/S0006-291X(67)80055-X.

590

591 **Figures and Tables**

592 **Figure 1. SAXS solution structure of BBK32-C/C1r-CCP2-SP. A)** Experimental SAXS curve
593 for the C1r-CCP2-SP/BBK32-C complex sample (black) shown with calculated theoretical SAXS
594 of the model (red) and residual plot below. A Guinier plot is shown inset. **B)** Normalized pair
595 distribution curves (P(r)) of C1r-CCP2-SP/BBK32-C complex (red), C1r-CCP2-SP (green), and
596 BBK32-C (blue). **C)** *Ab initio* SAXS envelope (gray) aligned with SAXS solution structure from
597 FoXSDock, refined with BILBOMD.

598 **Figure 2. SPR binding assays with structure-guided site-directed BBK32 mutants. A)** Surface
599 representations of BBK32-C and C1r-CCP2-SP denoted with non-contact surface areas (gray),
600 BBK32-C contact area (cyan), C1r-CCP2-SP contacts (green). Site-directed mutant contact
601 residues used for this study are denoted in red and were either single Ala mutations or double Ala
602 mutations as detailed in **Table S1**. **B)** To validate the C1r-CCP2-SP/BBK32-C complex observed
603 in the SAXS structure, SPR binding assays using BBK32-C site-directed mutants were performed.
604 A five-fold concentration series of C1r-CCP2-SP (0.8 to 500 nM) was injected over each
605 immobilized BBK32-C mutant. Surface plasmon resonance sensorgrams (black) with a kinetic fit
606 (red) show are shown. SPR experiments were performed in duplicate and dissociation constants
607 (K_D) are shown in red. Sensorgrams of additional mutants are presented (**Fig. S2**) and SPR
608 parameters are shown in **Table S1**.

609 **Figure 3. BBK32 R248 and K327 are critical for complement inhibitory activity of BBK32.**
610 **A)** ELISA-based complement activation assays were performed to determine the ability of
611 BBK32-C mutants to inhibit the classical pathway of complement *in vitro.* A two-fold
612 concentration series of each BBK32-C mutant was used and performed in duplicate. Inhibitory
613 data for additional site-directed mutants are presented in **Figure S4** and fitting parameters and

614 statistics are shown in **Table S1**. **B)** BBK32 mutant proteins were tested for their ability to confer
615 resistance to normal human serum (NHS). The serum sensitive strain B314 was transformed
616 separately with vector only (black), wildtype *bbk32* (blue), *bbk32*-R248A (red), *bbk32*-K327A
617 (green), and *bbk32*-R248A-K327A (purple) and incubated with NHS. Sensitivity was scored as a
618 ratio of the affected cells relative to the total cells viewed via darkfield microscopy. Heat
619 inactivated NHS was used as a control (right). P-values between *bbk32* samples are indicated
620 above. Statistical significance was assessed using a two-way ANOVA. **C)** The activation of
621 proenzyme C1s by full-length purified C1r was monitored by the cleavage of a C1s-specific
622 colorimetric substrate (Z-L-Lys-thiobenzyl) in the presence of 2,200 nM BBK32-C or BBK32-
623 R248A-K327A. Statistical significance was assessed using an unpaired t-test and the p-value is
624 reported.

625 **Figure 4. BBK32-C occludes the S1 and S1' subsites on C1r. A-B)** C1r-CCP2-SP shown with
626 the active site (yellow), substrate specificity subsites S1 (red) and S1' (blue) as determined by
627 Budayova and colleagues (33) using nomenclature provided by Schechter and Berger (62). The S1
628 site interacts with P1 residues on cognate peptide substrates and S1' site interacts with P1' residues,
629 with peptide hydrolysis occurring between the P1 and P1' residues. BBK32-C shown with residues
630 that contact the C1r S1 site (red) and S1' site (blue). By interacting with these sites, BBK32-C
631 effectively occludes the active site of C1r. **C)** Direct inhibition of C1r-CCP2-SP was assayed
632 using a small colorimetric peptide substrate, Z-Gly-Arg-thiobenzyl. A two-fold inhibitor
633 concentration series (1.1 – 2,200 nM) was performed with BBK32-C or BBK32-R248A-K327A.
634 BBK32-C was able to inhibit C1r-CCP2-SP, whereas the mutant was not.

635 **Figure 5. Comparison of BBK32 to gigastasin reveals convergent mechanisms of action.**
636 Ribbon diagrams of BBK32-C (PDB:6N1L), C1r-CCP2-SP (PDB:1MD8), Gigastasin/C1s-CCP2-

637 SP (PDB: 5UBM) with colored loop interactions within 4 Å, as judged by the program CCP4i
638 CONTACTS. The BBK32-C/C1r-CCP2-SP loop interactions are shown highlighted in red and
639 C1s/Gigastasin loop interactions in blue.

640 **Figure 6. C1r B loop residues contribute to enzymatic function. A)** A ribbon structure of the
641 BBK32/C1r-CCP2-SP complex is shown where BBK32-K327 is highlighted in cyan. The C1r B
642 loop is colored green and C1r residues making close contact with BBK32-K327 (i.e. N514, S516,
643 and D518) are highlighted. **B)** SPR-binding assay using immobilized BBK32-C and C1r-CCP2-
644 SP wild-type (solid line) or C1r-CCP2-SP-N514A-S516A-D518A (dashed line). Kinetic fits are
645 overlaid as red lines. **C)** SDS-PAGE-based proenzyme cleavage assay shows impaired cleavage
646 of the C1r substrate, proenzyme C1s, by C1r-CCP2-SP-N514A-S516A-D518A relative to wild-
647 type. Gel lane 1: proenzyme C1s control, 2: C1s enzyme control, 3: C1r-CCP2-SP + proenzyme
648 C1s, 4: C1r-CCP2-SP-N514A-S516A-D518A + proenzyme C1s. Gels were analyzed by
649 densitometry and data is shown on the right bar graph. A paired t-test was performed to determine
650 statistical significance and a p-value is shown. **D)** Enzymatic activation of proenzyme C1s by C1r-
651 CCP2-SP and C1r-CCP2-SP-N514A-S516A-D518A was determined by spectrophotometric assay
652 similar to the assay shown using full-length C1r in **Fig. 3C**. Data were analyzed using an unpaired
653 t-test to determine statistical significance and a p-value is shown.

654

655 **Table 1. MALS and SAXS parameters.**

Sample	Maximal dimension D_{max} (Å)	R_g (Å)	MW_{seq} (kDa)	MW_{SAXS} (kDa)	MW_{MALS} (kDa)	SAXS model fit χ^2
BBK32-C	~75	21.3 ± 0.9	16.9	19.9 ± 1.58	~19	2.08
C1r-CCP2-SP	~80	24.0 ± 0.9	37.7	31.7 ± 1.75	~40-60	1.06
BBK32-C/ C1r-CCP2-SP Complex	~85	27.8 ± 2.2	54.6	55.6 ± 4.13	~55-65	1.24

656

Fig. 1

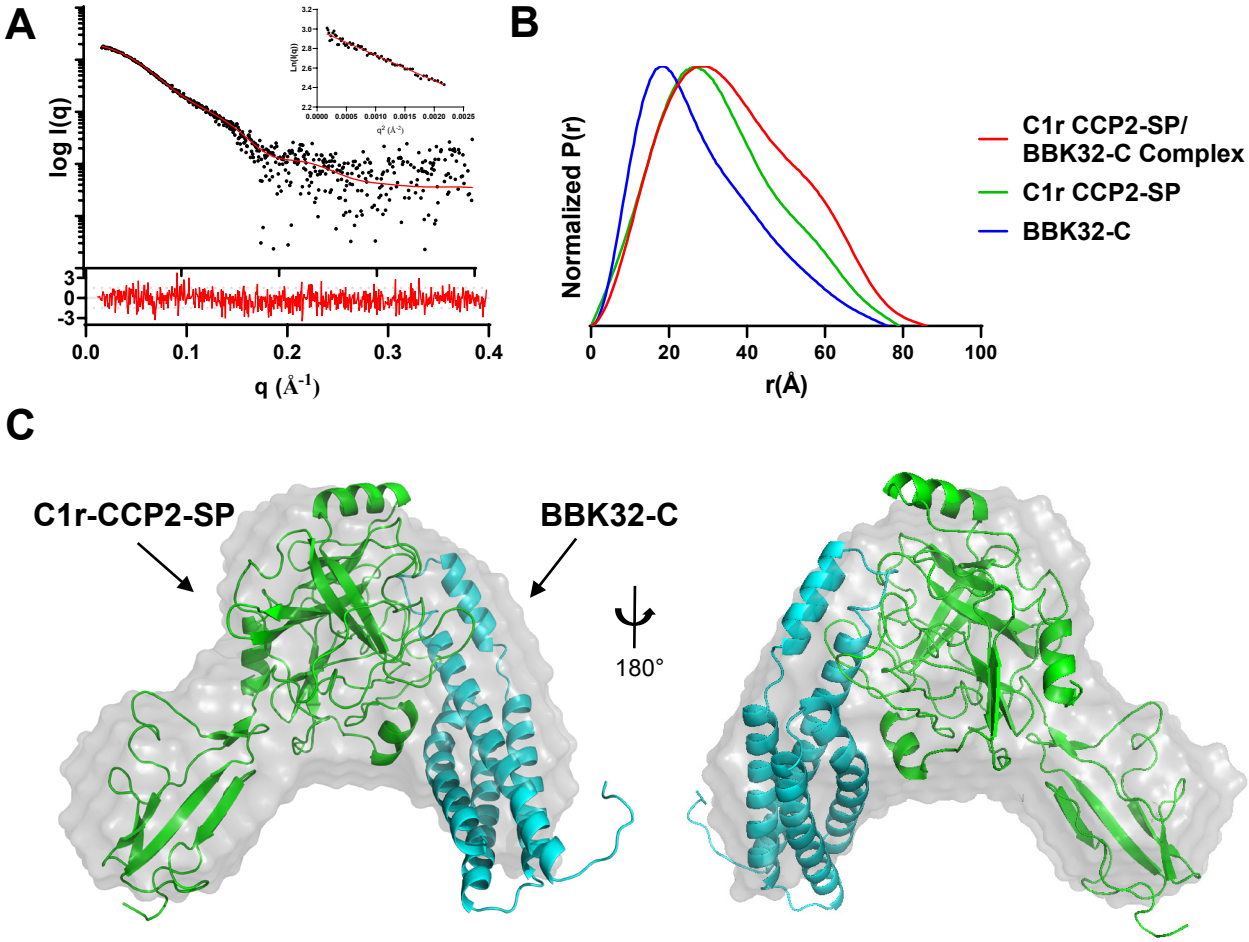
A
log I(q)
q (Å-1)
B
Normalized P(r)
r(Å)
C1r CCP2-SP/
BBK32-C Complex
C1r CCP2-SP
BBK32-C
C
C1r-CCP2-SP
BBK32-C
180°

Fig. 2

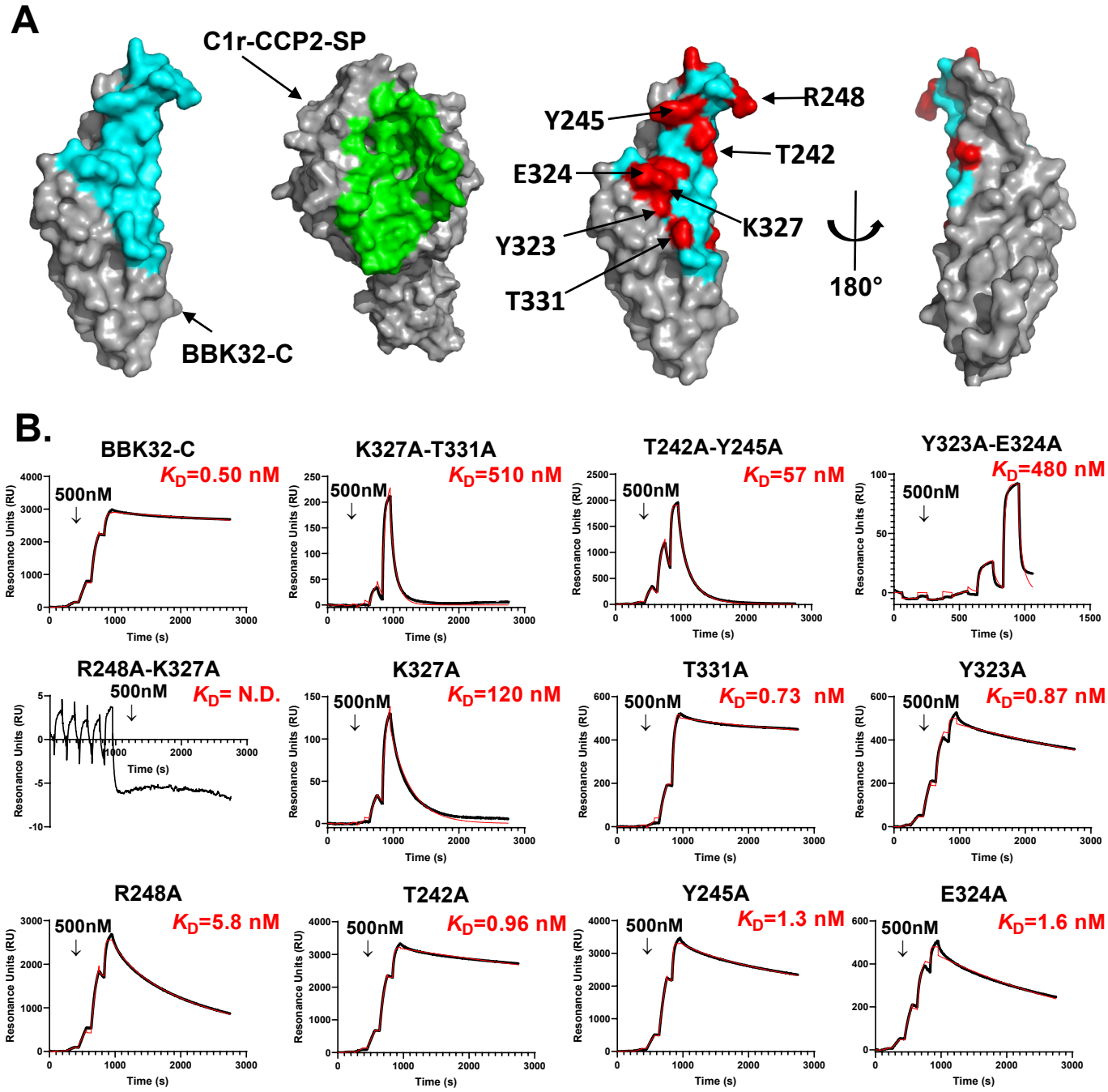
A
C1r-CCP2-SP
BBK32-C
Y245
R248
T242
E324
K327
Y323
T331
180°
B.
BBK32-C
K_D=0.50 nM
K327A-T331A
K_D=510 nM
T242A-Y245A
K_D=57 nM
Y323A-E324A
K_D=480 nM
R248A-K327A
K_D= N.D.
K327A
K_D=120 nM
T331A
K_D=0.73 nM
Y323A
K_D=0.87 nM
R248A
K_D=5.8 nM
T242A
K_D=0.96 nM
Y245A
K_D=1.3 nM
E324A
K_D=1.6 nM
500nM
Resonance Units (RU)
Time (s)

Fig. 3

A

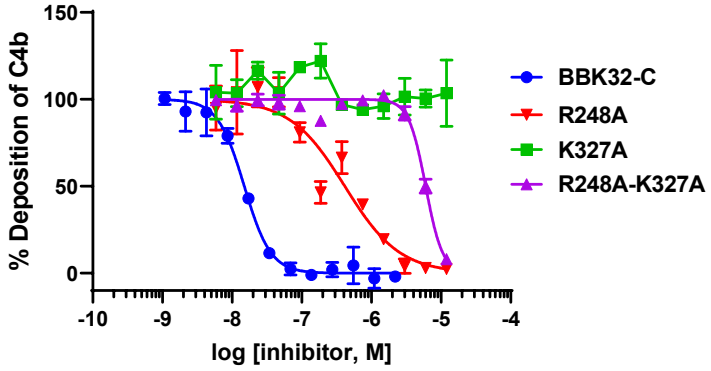
% Deposition of C4b
150
100
50
0
-10
-9
-8
-7
-6
-5
-4
log [inhibitor, M]
BBK32-C
R248A
K327A
R248A-K327A

B

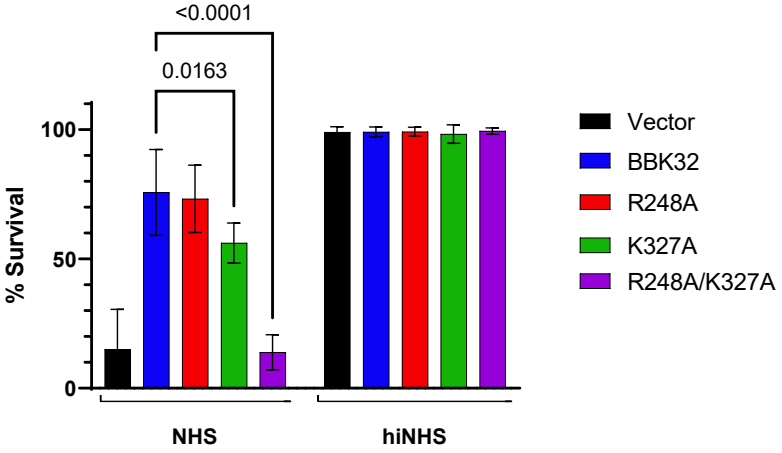
<0.0001
0.0163
% Survival
100
50
0
NHS
hiNHS
Vector
BBK32
R248A
K327A
R248A/K327A

C

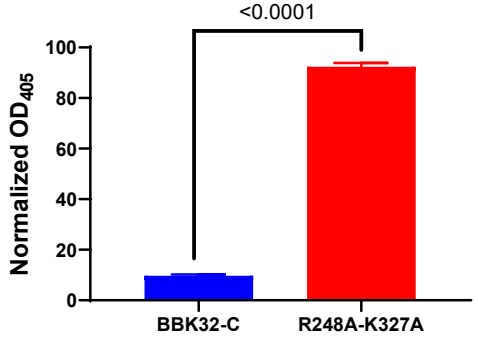
<0.0001
Normalized OD_{405}
100
80
60
40
20
0
BBK32-C
R248A-K327A

Fig. 4

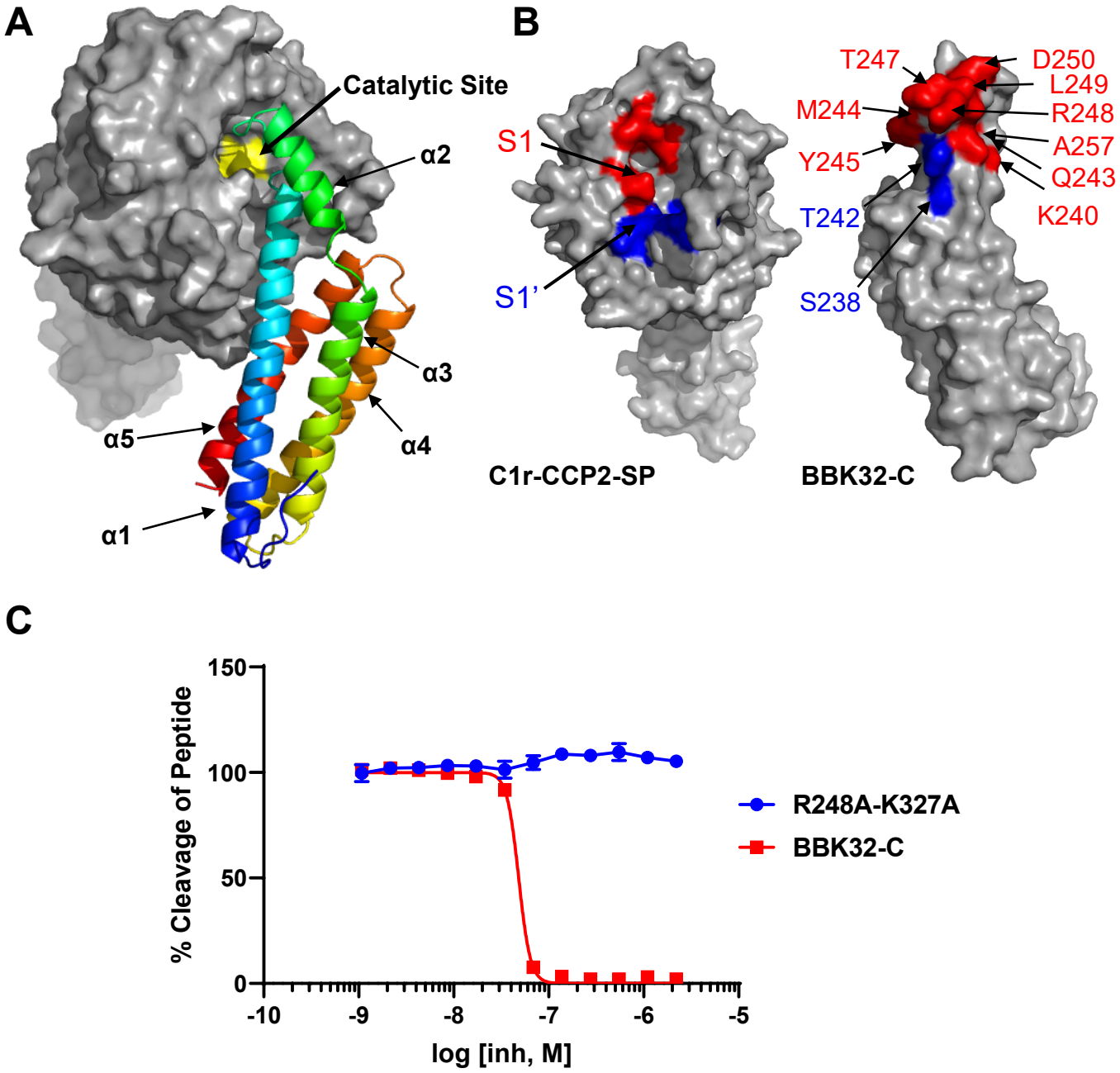
A
Catalytic Site
α2
α3
α4
α5
α1
B
S1
S1'
C1r-CCP2-SP
T247
D250
L249
M244
R248
A257
Y245
Q243
T242
K240
S238
BBK32-C
C
% Cleavage of Peptide
150
100
50
0
-10
-9
-8
-7
-6
-5
log [inh, M]
R248A-K327A
BBK32-C

Fig. 5

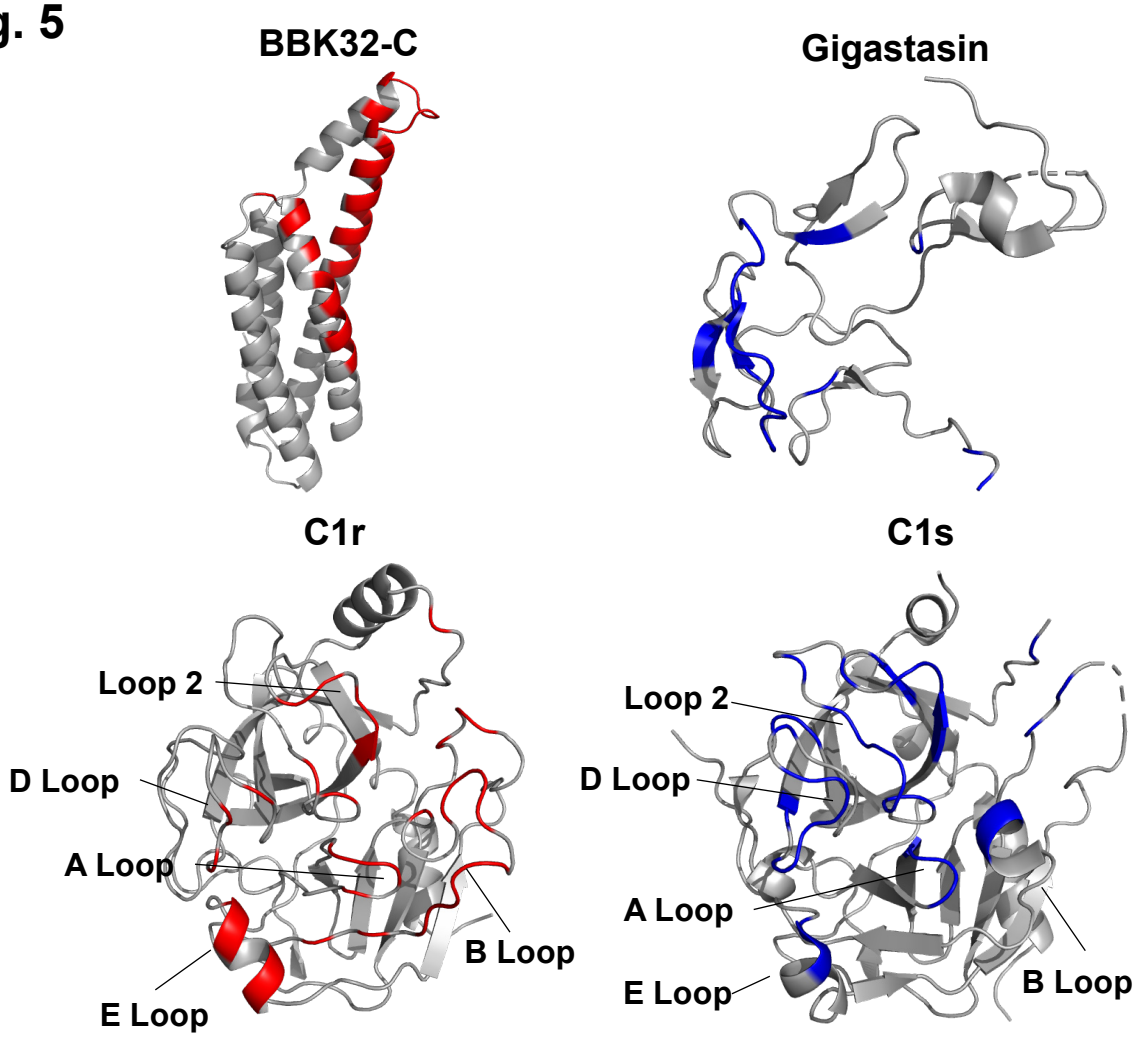


```
                                A Loop                                  B Loop                  E Loop
C1r  IIGGQKAKMGNFPWQVFTNIHGRGGGALLGDRWILTAAHTLYPKEHEAQSNASLDVFLGHTNVEE--LMKLGNHPIRRVS
C1s  IIGGSDADIKNFPWQVFFDNP-WAGGALINEYWVLTAAHVVEGNRE-------PTMYVGSTSVQTSRLAKSKMLTPEHVF
     ****..*.: ******* :    .****:.: *:*****.:  :..         :::* *.*:   * *      .:*
                C Loop                                                          D Loop
C1r  VHPDYR----QDESYNFEGDIALLELENSVTLGPNLLPICLPDNDTFYDL--GLMGYVSGFGVMEEK-IAHDLRFVRLPV
C1s  IHPGWKLLEVPEGRTNFDNDIALVRLKDPVKMGPTVSPICLPGTSSDYNLMDGDLGLISGWGRTEKRDRAVRLKAARLPV
     :**.::     :   **:.*a***:.*:: *.:**.: *****...: *:* * :* :**:*  *::  *  *: .****
                                                Loop 1                                  Loop 2
C1r  ANPQACENWLRGK----NRMDVFSQNMFCAGHPSLKQDACQGDSGGVFAVRDPNT-DRWVATGIVSWGIGCSRGYGFYTK
C1s  APLRKCKEVKVEKPTADAEAYVFTPNMICAGGE-KGMDSCKGDSGGAFAVQDPNDKTKFYAAGLVSWGPQCG-TYGLYTR
     *  : *::    *     .  **: **:***      *:*:*****.***:***   :: *:*:****  *.  **:**:

C1r  VLNYVDWIKKEMEEED-----
C1s  VKNYVDWIMKTMQENSTPRED
     * ****** * *:*:.
```

Fig. 6

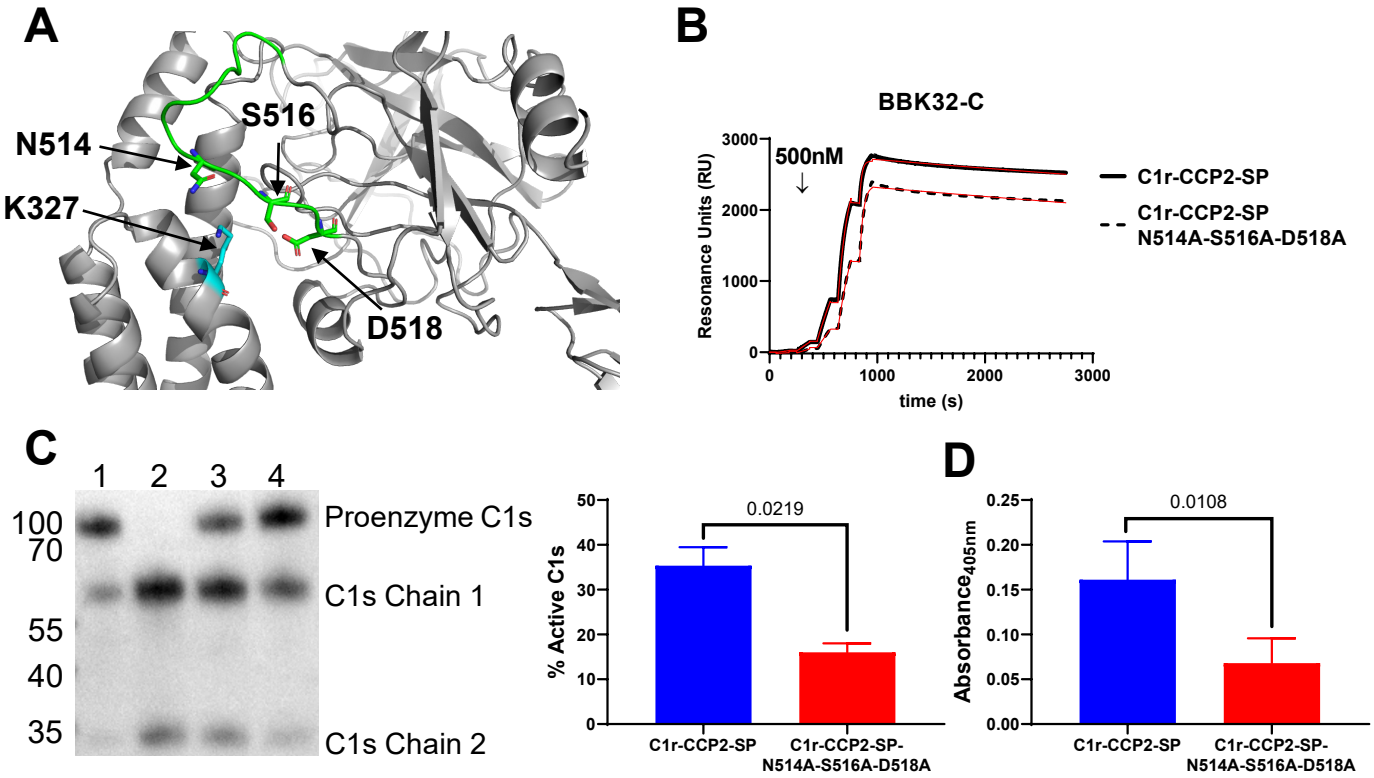
A
N514
S516
K327
D518
B
BBK32-C
500nM
Resonance Units (RU)
3000
2000
1000
0
0
1000
2000
3000
time (s)
C1r-CCP2-SP
C1r-CCP2-SP
N514A-S516A-D518A
C
1
2
3
4
100
70
55
40
35
Proenzyme C1s
C1s Chain 1
C1s Chain 2
% Active C1s
50
40
30
20
10
0
0.0219
C1r-CCP2-SP
C1r-CCP2-SP-
N514A-S516A-D518A
D
Absorbance405nm
0.25
0.20
0.15
0.10
0.05
0.00
0.0108
C1r-CCP2-SP
C1r-CCP2-SP-
N514A-S516A-D518A